Pattern formation of ion channels with state-dependent charges and diffusion constants in fluid membranes

Stephan C. Kramer and Reiner Kree
Institut für Theoretische Physik, Georg-August-Universität Göttingen, Bunsenstrasse 9, 37073 Göttingen
(Received 25 October 2001; published 17 May 2002)

A model of mobile, charged ion channels in a fluid membrane is studied. The channels may switch between an open and a closed state according to a simple two-state kinetics with constant rates. The effective electrophoretic charge and the diffusion constant of the channels may be different in the closed and in the open state. The system is modeled by densities of channel species, obeying simple equations of electrodiffusion. The lateral transmembrane voltage profile is determined from a cable-type equation. Bifurcations from the homogeneous, stationary state appear as hard-mode, soft-mode, or hard-mode oscillatory transitions within physiologically reasonable ranges of model parameters. We study the dynamics beyond linear stability analysis and derive nonlinear evolution equations near the transitions to stationary patterns.

DOI: 10.1103/PhysRevE.65.051920 PACS number(s): 87.10.+e, 87.16.Ac, 87.16.Uv

I. INTRODUCTION

Spontaneous pattern formation of ion channels in cell membranes has been a subject of continuous interest during recent years [1–4]. Spatially modulated distributions of ion channels or pumps are ubiquitous in biological cells and they are closely related to important biological functions like morphogenesis [5] or storage and processing of information in neural tissue [6]. Many physiological regulation processes involve changes of ion fluxes through cell membranes on time scales ranging from milliseconds to hours [5,6].

There have been attempts to explain the aggregation of channel proteins in a fluid membrane on the basis of thermodynamic models [7,8], but typically the system of channels is driven out of equilibrium due to ionic concentration gradients and transmembrane fluxes. Therefore, a number of authors have put forward models for spontaneous pattern formation based upon semiphenomenological, nonequilibrium equations of motion for the densities of channel proteins. The open channels cause transmembrane ion currents and are coupled to the voltages near the membrane surface, if they carry a charge. Thus the models have to be completed by equations that determine the ion transport (Nernst-Planck equations) and by the Poisson equation of electrodynamics. They have to be supplemented with boundary conditions, which take into account the dielectric nature of the lipid membrane [1,9,3,4].

These electrodiffusive models can be applied to a number of important systems like axons or closely neighboring cells in tissue. In such systems there is a thin layer of electrolyte (10–100 nm) on one side of the membrane and a bulk reservoir of ions in aqueous solution on the other side. The Ohmic resistance of the thin layer cannot be neglected and ionic fluxes within the layer, caused by transmembrane currents, give rise to significant lateral voltage drops, which are absent on the reservoir side of the membrane (see Fig. 1 for a schematic picture).

The electrodiffusive models are frequently used in a simplified form, where ion densities are approximately eliminated from the equations. Then the lateral voltage profile is determined from a quasi one-dimensional or two-dimensional cable equation [2,10,11], which leads to an effective coupling between channels caused by their associated transmembrane currents.

During the process of elimination of ions, the electroosmotic drift of channel proteins due to ion motion within the Debye layers near charged lipid surfaces leads to a renormalization of the effective electrophoretic charge of the channels, as has been shown in [4]. Depending on size and conformation, negatively charged channel proteins may even appear as positively charged due to this effect.

Electrodiffusive models of the above type contain a simple mechanism, which may drive pattern formation [1]. It is based on a feedback loop during which the channel pro-

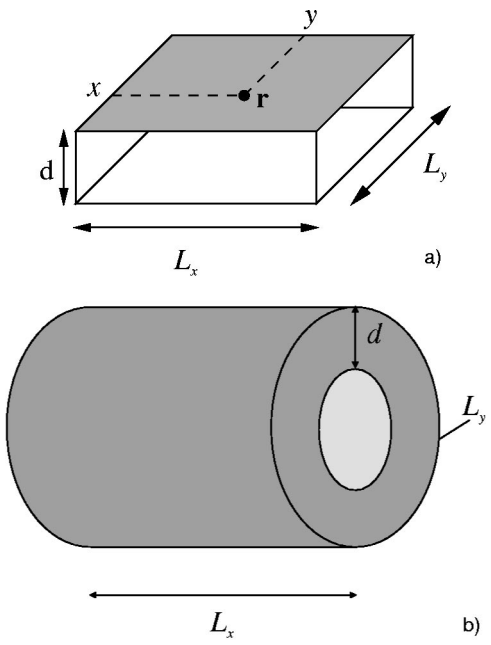

FIG. 1. (a) Model geometry of membrane patch $L_x \times L_y$ (shaded), separated from an inert surface by a cleft of width d. (b) Same model geometry with periodic boundary condition in the y direction.

teins drift due to lateral voltage gradients and at the same time modify these voltage gradients by Ohmic voltage drops caused by transmembrane currents. Therefore, for example, negatively charged channels (drifting in the direction of increasing voltage), which cause currents directed into the thin layer of electrolyte, have a tendency to aggregate, because the currents will lead to a further increase of voltage. Diffusion will counteract this tendency by dispersing the channels. Bifurcations of the homogeneous state to an inhomogeneous state may be possible if drift currents become big enough to overcome diffusion, provided the channels are always open and do not change their properties that determine their diffusion and effective electrophoretic charge.

In reality, however, ion channels involved in signal transmission and regulation processes will switch between a variety of conformations or molecular complexes corresponding to closed as well as open states. The different conformations and complexes may have different diffusion constants and effective electrophoretic charges. Typical examples, which cause state dependencies of diffusion and charge are charge transport across the lipid membrane [12–14] and immobilization due to binding to the cytoskeleton [14,15].

In the present work, we will set up and analyze a minimal generic model for mobile channels with internal state kinetics, which includes state-dependent diffusion and charge of the ion channels. For simplicity and lucidity, we will only consider a simple two-state kinetics (reactions connecting one open and one closed state) with constant rates. This allows for a fairly complete discussion of the first bifurcations from the homogeneous and stationary state of the channel densities and the voltage.

Special cases of such a model have been studied previously. In Ref. [2] the authors considered open channels in chemical exchange with a reservoir of closed channels. This reservoir is treated in the well-stirred approximation without coupling to the lateral voltage profile. Thereby the model reduces to an electrodiffusive model with one channel type, but the particle number of these channels is no longer conserved. We will see below that our model leads to qualitatively different behavior in a wide range of parameters but still contains the results of [2]. The necessary limit is that of closed channels, which diffuse much faster than the open ones and possess vanishing electrophoretic charge. The present model is also related to [16], where a mixture of two different channel types has been considered, but without reactions, which allow for transitions between the different species.

After introducing the model in the following section, we will give our results of the linear stability analysis. Depending on parameter ranges either soft-mode instabilities arise (periodic patterns appear with a wave number k_c, which approaches zero at the transition) or there will be different kinds of hard-mode instabilities, where patterns with $k_c \neq 0$ occur at the transition. We also will find the emergence of spatiotemporal patterns with nonvanishing k_c and nonvanishing frequency Ω_c. In Sec. IV we will derive results of the nonlinear behavior of our model close to transitions into stationary patterns. For soft-mode instabilities, we will find a Cahn-Hilliard-type equation of motion for slow modes near the transition. For hard-mode instabilities, an amplitude equation will be derived, which allows us to separate parameter regions leading to continuous transitions from those leading to discontinuous transitions. Details of the derivation of the nonlinear evolution equations will be presented in two appendices.

II. THE MODEL

We consider ion channels moving within a fluid membrane of size $L_x \times L_y$, which separates a thin layer of electrolyte of width d from an electrolytic bath, as it is sketched in Fig. 1. Positions $\mathbf{r}$ within the membrane are described by internal rectilinear coordinates $\mathbf{r}=(x,y)$, $0 \leqslant x < L_x$, $0 \leqslant y < L_y$. We will be interested in infinitely extended systems (L_x, $L_y \to \infty$), such that we can neglect boundary and geometry effects in the following discussion. We merely mention that if we choose periodic boundary conditions in the y coordinate, the membrane corresponds to a cylindrical cable and is reminiscent of axonic or dendritic structures for $L_x >> L_y$. Note that we treat L_y and d as independent quantities, so that the actual structure in cylindrical geometry looks like Fig. 1(b), with a submembrane layer of width d and a "core" of radius $(L_y/2\pi)-d$, which is decoupled from the submembrane layer. For $d=L_y/2\pi$ the submembrane layer fills the entire interior of the cable. A more detailed analysis of boundary effects and the influence of different geometries will be given elsewhere [17].

Ion channels may switch between an open state (o) and a closed state (c) according to a simple monomolecular chemical reaction scheme

$$\begin{array}{c} \gamma_+ \\ \downarrow \\ c \rightleftharpoons o \\ \uparrow \\ \gamma_- \end{array} \qquad (1)$$

with rates γ_- and γ_+. We are interested in a wide range of kinetic rates, from 10^3/sec for voltage or ligand gated channels down to less than one per hour as is observed for hormone regulated phosphorylation and dephosphorylation of channel proteins. For gated channels, the rates depend on voltage and/or ligand concentration, but within our simplest, generic model we will treat $\gamma_\pm$ as constants. We will see below that voltage dependencies will not modify the linear stability analysis. Temporal variations of ligand concentration provide a distinct external driving mechanism, which will be studied elsewhere [17]. The distribution of channels is described by smooth densities $n_r(\mathbf{r},t), r \in \{o, c\}$, which obey the equations

$$\partial_t n_r(\mathbf{r},t) + \boldsymbol{\nabla} \cdot \mathbf{j}_r(\mathbf{r},t) = \sigma_r [\gamma_+ n_c(\mathbf{r},t) - \gamma_- n_o(\mathbf{r},t)] \qquad (2)$$

with $\sigma_r=+1$ for $r=o$ and $\sigma_r=-1$ for $r=c$. The right-hand side of this equation takes into account the reaction kinetics of Eq. (1). Current densities $\mathbf{j}_r$ of the channels are assumed to be of the Nernst-Planck form

$$\mathbf{j}_r(\mathbf{r},t)=-D_r\{\boldsymbol{\nabla} n_r(\mathbf{r},t)-\beta q_r n_r(\mathbf{r},t)\mathbf{E}(\mathbf{r},t)\}, \tag{3}$$

where D_r and q_r refer to the constants of lateral diffusion and to the effective electrophoretic charges of open and closed channels, respectively.

The coefficient β is the inverse temperature and $\mathbf{E}(\mathbf{r})=-\boldsymbol{\nabla} V(\mathbf{r})$ denotes the lateral electric field. Note that we explicitly allow for different diffusion constants and different electrophoretic charges in the states o and c.

The simple form of the current densities given in Eq. (3) may be justified for rigid protein structures with charged protuberances extending in the intracellular and extracellular electrolyte. As discussed in [4], the effective electrophoretic charges may be of both signs due to electro-osmotic effects, although proteins are usually negatively charged.

The Kelvin cable equation or its two-dimensional analog may be used to calculate the lateral variation of the transmembrane potential provided that spatial variations of ion concentrations have negligible effects and that the characteristic length scales of lateral patterns are large compared to the width of the thin layer of the electrolyte. A careful discussion of the derivation of the cable equation from the Nernst-Planck theory can be found in [11]. In the following we will use the two-dimensional cable equation [2]

$$C_m\partial_t V(\mathbf{r},t)=\frac{d}{\rho_e}\nabla^2 V(\mathbf{r},t)-GV(\mathbf{r},t) -\lambda n_o(\mathbf{r},t)\{V(\mathbf{r},t)-E\}. \tag{4}$$

C_m denotes membrane capacitance per area, ρ_e is the resistivity of the electrolyte within the thin layer of width d, and λn_o is the conductance of open channels. We have included a passive, homogeneously distributed transmembrane conductance G. E is the reversal potential of ion fluxes through the open channels, which drives the system out of equilibrium.

We are interested in the stability of the homogeneous and stationary solution $\overline{V},\overline{n_o},\overline{n_c}$ of Eqs. (2)–(4),

$$\overline{V}=\frac{\lambda\overline{n_o}E}{G+\lambda\overline{n_o}},$$

$$\overline{n_o}=\frac{\gamma_+}{\Gamma}\overline{n}, \quad \overline{n_c}=\frac{\gamma_-}{\Gamma}\overline{n}. \tag{5}$$

The total density of channels, $\overline{n}=\overline{n_o}+\overline{n_c}$, is constant and we define $\Gamma:=\gamma_++\gamma_-$. To prepare the following analysis, we introduce appropriately normalized deviations from the stationary and homogeneous solution as the new fields $\rho=(n_o-\overline{n_o})/\overline{n_o}$, $\zeta=(n_c-\overline{n_c})/\overline{n_c}$, and $\Phi=\beta q_o(V-\overline{V})/\overline{V}$. We change to dimensionless lengths and times by using as units the typical decay length of V, $\ell_V=[(\rho_e/d)(\lambda\overline{n_o}+G)]^{-1/2}$, and a typical diffusion time over this length $\tau=\ell_V^2/D_o$. Then Eqs. (2)–(4) take on the dimensionless form

$$\partial_t\varrho=\boldsymbol{\nabla}\cdot\{\boldsymbol{\nabla}\varrho+(\varrho+1)\boldsymbol{\nabla}\Phi\}-\gamma_-(\varrho-\zeta), \tag{6}$$

$$\partial_t\zeta=D\boldsymbol{\nabla}\cdot\{\boldsymbol{\nabla}\zeta+q(\zeta+1)\boldsymbol{\nabla}\Phi\}+\gamma_+(\varrho-\zeta), \tag{7}$$

$$\epsilon\partial_t\Phi=[\nabla^2-1]\Phi-\alpha\Phi\varrho-\eta\varrho. \tag{8}$$

In these equations we use the reduced parameters $D=D_c/D_o$, $q=q_c/q_o$, $\alpha=\lambda\overline{n_o}/(\lambda\overline{n_o}+G)$, and $\eta=-\alpha(1-\alpha)\beta q_o E$. The parameter $\epsilon=C_m\rho_e D_o/d$ compares the electrical relaxation (RC) time per area to the diffusion constant. Note that γ_+ and γ_- have also been made dimensionless by multiplication with τ ($\gamma_\pm\to\gamma_\pm\tau$).

For cell membranes, the parameters in Eqs. (2)–(4) imply time scales, which differ by several orders of magnitude. According to [12], typical parameter values are $C_m=1\ \mu\mathrm{F/m^2}$, $\rho_e\sim 1\ \Omega\,\mathrm{m}$, $d\sim 10$ nm, and $D_r\sim 0.1\ (\mu\mathrm{m})^2/\mathrm{sec}$ for diffusion of mobile proteins. Channel conductances λ are in the $10^{-12}\ \Omega^{-1}$ range, average channel densities are around 10–50 $\mu\mathrm{m}^{-2}$, and electrotonic lengths ℓ_V are of the order of a few microns. Then the unit of time $\tau\sim 10^2$ sec, whereas the electrical (RC) relaxation time is below 1 μsec. This is always the smallest time scale of the system, even compared to fast kinetics of voltage or ligand gated channels with time constants in the millisecond range. The constant $\epsilon\sim 10^{-7}$. This separation of time scales justifies the use of the quasistationary approximation in Eq. (8) and hence in the following we will put the rhs of Eq. (8) equal to zero. For voltage or ligand gated channels, the time scale set by the rate Γ is also very fast compared to τ, $\Gamma\sim 10^5$, whereas slower regulation processes have time scales comparable to or larger than τ. The limit $\Gamma\gg 1$, $\gamma_+/\gamma_-=O(1)$ will be referred to as the *fast reaction limit* in the following.

For reversal potentials $|E|\sim 0$–100 mV and electrophoretic charges of a few elementary units, the parameter η is in the range $|\eta|\sim 0$–10 under physiological conditions.

III. LINEAR STABILITY ANALYSIS

We linearize Eqs. (6)–(8) around the homogeneous and stationary solution, Eq. (5), and apply the plane wave ansatz $(\varrho,\zeta,\Phi)=(\varrho_k,\zeta_k,\Phi_k)\exp\{i\mathbf{k}\cdot\mathbf{x}+\omega t\}+\mathrm{c.c.}$

Within the quasistationary approximation potential fluctuations Φ_k are proportional to fluctuations of open channels

$$\Phi_k=-\eta\varrho_k/(1+k^2). \tag{9}$$

Inserting Eq. (9) into the linearized Eqs. (6) and (7) we get the eigenvalue problem

$$\omega\begin{pmatrix}\varrho_k\\ \zeta_k\end{pmatrix}=\left\{\begin{pmatrix}-\gamma_- & \gamma_-\\ \gamma_+ & -\gamma_+\end{pmatrix}-k^2\begin{pmatrix}1-\eta_k & 0\\ -Dq\,\eta_k & D\end{pmatrix}\right\}\begin{pmatrix}\varrho_k\\ \zeta_k\end{pmatrix} \tag{10}$$

with $\eta_k=\eta/(1+k^2)$. The eigenvalues

$$\omega_\pm=-[P(k^2)\pm\sqrt{Q(k^2)}]/2,$$

$$P(k^2)=k^2(1+D-\eta_k)+\Gamma,$$

$$Q(k^2)=[k^2(1-D-\eta_k)+\gamma_- -\gamma_+]^2+4Dq\gamma_- k^2\eta_k + 4\gamma_-\gamma_+ \tag{11}$$

determine linear stability. Let us note that an extended model with voltage dependent reaction rates will lead to the same set of linearized equations.

The solution (5) becomes unstable against small perturbations if $\mathrm{Re}\,\omega_+$ or $\mathrm{Re}\,\omega_-$ is positive. Note that oscillatory unstable modes, which require $\mathrm{Im}\omega_\pm\neq 0$ (and thus $Q<0$) are possible in the parameter range $q\eta<0$.

The influence of the parameters η and q on the qualitative behavior of solutions is already apparent in the nonlinear system, Eqs. (6)–(8). The term $\eta\varrho$ in Eq. (8) drives the curvature of the potential Φ, whereas q may change the direction of drift currents of the closed channels relative to their diffusion currents and to the drift currents of the open channels. For example, if open cation channels carry a negative charge, they drift in the direction of increasing V. If the reversal potential $E<0$ is such that the cation current through open channels $\lambda n_o(V-E)$ is directed into the thin layer of electrolyte, this current will lead to a further increase of V and may cause an enhanced aggregation of open channels. If closed channels have a positive effective electrophoretic charge, the accumulated open channels will disperse again after closing. This may lead to an oscillatory behavior. By varying the relative signs of q and η, different scenarios of aggregation and dispersion of channels by lateral structures in Φ may arise, which are coupled back into Eq. (8) and may lead to stationary or oscillatory patterns.

In the following we will hence discuss the four parameter regions $\mathcal{R}_{++}$ $(q>0,\eta>0)$, $\mathcal{R}_{--}$ $(q<0,\eta<0)$, $\mathcal{R}_{+-}$ $(q>0,\eta<0)$, and $\mathcal{R}_{-+}$ $(q<0,\eta>0)$ separately. The quantity η is treated as the primary control parameter.

A. Instabilities for $q\eta>0$

In the regions $\mathcal{R}_{++}$ and $\mathcal{R}_{--}$, $Q(k^2)$ is always positive, the rates $\omega_\pm(k^2)$ are real and thus plane wave solutions will either exponentially grow or decay in time. Instabilities signal the onset of stationary patterns. As $\omega_+>\omega_-$, it is the rate ω_+, which will drive the solution (5) unstable, if control parameters reach the stability boundary. Note that in the long-wavelength limit $k\to 0$, $\omega_+=O(k^2)$ and thus vanishes for all values of $\eta,q,D,\gamma_\pm$. The corresponding diffusion mode reflects conservation of the total number of channels.

From $\omega_+\omega_-=0$ we get the neutrality condition

$$\eta_0(k)=(1+k^2)\frac{D(k^2+\gamma_-)+\gamma_+}{D(k^2+q\gamma_-)+\gamma_+}. \tag{12}$$

The minimum of $\eta_0(k)$ corresponds to the first onset of instabilities and the corresponding wave number k_c is the first unstable mode (critical mode). A minimum of the neutral curve appears at $k_c\neq 0$ with

$$k_c^2=-q\gamma_- -\frac{\gamma_+}{D}+\sqrt{\gamma_-(q-1)(q\gamma_-+\gamma_+/D-1)} \tag{13}$$

if the rhs of Eq. (13) is a positive, real number. By varying q,D or the rates $\gamma_\pm$, the instability may switch between soft-mode $(k_c=0)$ and hard-mode $(k_c\neq 0)$ type.

Several statements are noticeable.

(a) For $D=0$, (immobile closed channels), as well as for $q=1$, the neutrality condition $\eta_0=1+k^2$ is independent of the reaction rates and implies a soft-mode instability at $\eta_c=1$. A hard-mode instability requires both mobile channels and different charges of closed and open states.

(b) Hard-mode instabilities are only possible for $q=q_c/q_o<1$, i.e., $q_c<q_o$. Especially if $0<q<1$, then obviously $|q_c|<|q_o|$.

(c) For $D\to\infty$ and $Dq=0$ we recover the results of [2].

(d) In the fast reaction limit only soft-mode instabilities at $\eta_c=(D\gamma_-/\gamma_+ +1)/(Dq\gamma_-/\gamma_+ +1)$ remain. Note that the critical control parameter stays small $[O(1)]$ in the fast reaction limit, indicating that the instability may indeed be reached under physiological conditions.

For reaction rates $O(1)$, typical curves of $\eta_0(k)$ are shown in Fig. 2. In $\mathcal{R}_{++}$, both soft- and hard-mode instabilities may occur. In $\mathcal{R}_{--}$ a neutral curve only appears for $D|q|>\gamma_+/\gamma_-$. Then $\eta_0(k)$ is maximal at $k=0$ and exhibits poles at $k_p^2=-q\gamma_- -\gamma_+/D$. Thus, for electrophoretic charges q_o,q_c of different signs and $\eta<0$, merely soft-mode instabilities are possible [Fig. 2.(b)]. Note that only a finite band of unstable modes, limited to the interval $(-k_p,k_p)$, will appear for all $\eta<0$. This unstable band grows like $k_p\sim\Gamma^{1/2}$ in the fast reaction limit. Figure 3 shows the $k_c^2=0$ lines in the $D-\Gamma$ plane for different values of q. For parameters (D,Γ) below each curve $k_c^2>0$.

Solving the linearized system for the eigenvector $(\varrho_{k_c},\zeta_{k_c},\Phi_{k_c})$ of the critical mode with $\varrho_{k_c}=1$, one gets $\zeta_{k_c}=(qk_c^2+q\gamma_-+\gamma_+/D)/(k_c^2+q\gamma_-+\gamma_+/D)$ and $\Phi_{k_c}=-(k_c^2+q\gamma_-+\gamma_+/D)/(k_c^2+q\gamma_-+\gamma_+/D)$. Thus $\mathrm{sgn}\,\varrho_{k_c}=\mathrm{sgn}\,\zeta_{k_c}$ and $\mathrm{sgn}\,\varrho_{k_c}=-\mathrm{sgn}\,\Phi_{k_c}$ if $q>0$. Hence for $q>0$, spatial variations of open and closed channels are in phase but have a phase lag of π with respect to the potential in the critical mode. If $q<0$ there is no phase lag, as then $\mathrm{sgn}\,\omega_{k_c}=\mathrm{sgn}\,\zeta_{k_c}=\mathrm{sgn}\,\Phi_{k_c}$. In this case the critical wave number vanishes leading to $\zeta_0=1$ and $\Phi_0=-\eta_c$ so that all spatial periods are in phase as expected from the qualitative discussion on the mechanism of pattern formation given in Sec. II after Eq. (8).

B. Instabilities for $q\eta<0$

The simplest behavior of the system appears in the regime $\mathcal{R}_{+-}$. For $\mathrm{Im}\,\omega_\pm\neq 0$, it is obvious from Eq. (11) that $\mathrm{Re}\,\omega_\pm=-(1/2)P(k^2)<0$. It is easy to show that linear stability also holds for $\mathrm{Im}\,\omega_\pm=0$ and thus the homogeneous, stationary solution (5) is linearly stable in this regime.

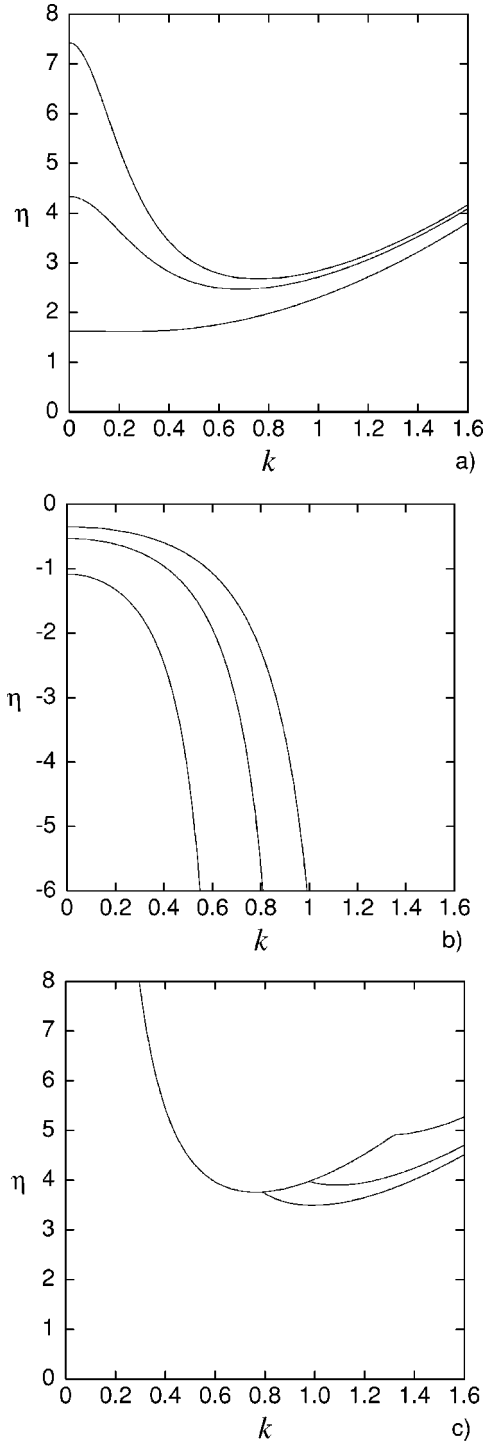

FIG. 2. Neutral curves in regions $\mathcal{R}_{++}$ (a), $\mathcal{R}_{--}$ (b), and $\mathcal{R}_{-+}$ (c) for different values of q. For the upper, middle, and lower curves, $q=0.1$, 0.2, and 0.6 in (a); $q=-3.0$, -2.0, and -1.0 in (b); and $q=-0.3$, -0.5, and -1.0 in (c). Other parameters are $\gamma_+=0.01$, $\gamma_-=0.5$, and $D=0.5$.

$\mathcal{R}_{-+}$ is the only parameter regime, where oscillatory instabilities may occur, because $Q(k^2)$ and $P(k^2)$ can simultaneously take on negative values in this regime. If $Q<0$, $\omega_+=\omega_-^*$ and the growth rate of the perturbation is $\mathrm{Re}\,\omega_\pm=-P(k^2)/2$. From $P(k^2,\eta)=0$ we obtain the neutrality condition $\eta_P(k)$ for oscillatory instabilities,

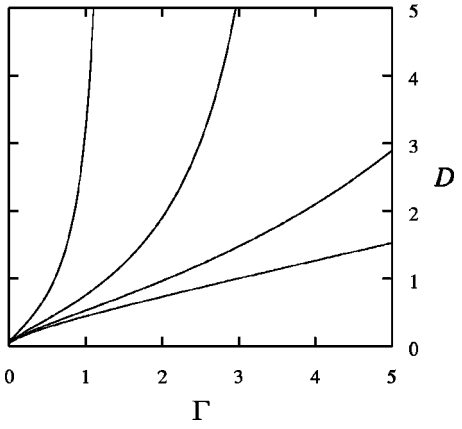

FIG. 3. Boundaries between hard-mode and soft-mode instabilities in D-γ plane in $\mathcal{R}_{++}$ for different values of q. In regions below each curve, $k_c^2>0$. From lower to upper curves, values of q are 0.0, 0.1, 0.25, and 0.5.

$$\eta_P(k)=(1+D)(1+k^2)\left(1+\frac{\Gamma}{(1+D)k^2}\right). \tag{14}$$

It attains its minimum at the critical wave number $k_{P_c}=\sqrt[4]{\Gamma/(1+D)}$. The critical value of the control parameter is

$$\eta_{P_c}=(1+D)\left(1+\sqrt{\frac{\Gamma}{1+D}}\right)^2. \tag{15}$$

Note that $P(k^2)$ and hence the neutral curve do not depend on the ratio q of the electrophoretic charges. The ratio q will enter in the oscillation frequency $\Omega_c=(1/2)\sqrt{|Q(k_c^2)|}$ at the critical point.

The region $\mathcal{R}_{-+}$ also contains parts with $Q(k^2)>0$, where stationary unstable patterns may arise if the neutral curve determined from Eq. (12) is crossed. Hence the true critical point is located at

$$\eta_c=\min_k\{\eta_0(k),\eta_P(k)\}. \tag{16}$$

Figure 2(c) shows neutral curves in $\mathcal{R}_{-+}$ for different values of q. Generically a neutral curve in $\mathcal{R}_{-+}$ is composed of two branches. The one belonging to the onset of oscillatory instabilities does not depend on q, whereas the other one—belonging to stationary patterns—does. By increasing $|q|$ or D (see Fig. 4) η_c changes discontinuously from an instability with $\Omega_c>0$ to an instability towards stationary patterns.

The dependence of Ω_c on Γ and D is depicted in Fig. 5. Oscillatory instabilities will not be attainable in the fast reaction limit under physiological conditions because $\eta_{P_c}\sim\Gamma$ for large Γ.

Figure 4 shows neutral curves in $\mathcal{R}_{-+}$ together with the region $Q(k^2)<0$ for two cases, which differ by the value of D. In Fig. 4(a), the unstable pattern is oscillating, in Fig. 4(b), it is stationary. Figure 5 shows the dependence of the

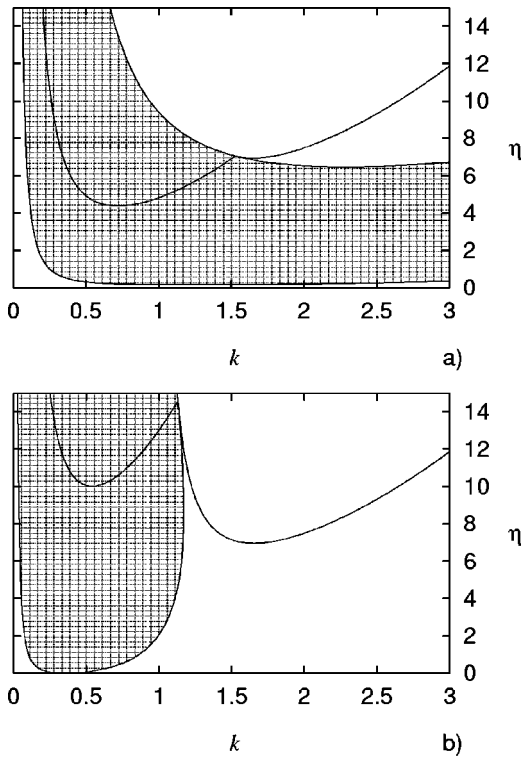

FIG. 4. Neutral curves and domain of complex eigenvalues (shaded) in $\mathcal{R}_{-+}$ for $D=0.09$ (a) and $D=5.0$ (b). Note that there is a discontinuous change in the nature of the transition with increasing D; from hard-mode stationary to hard-mode oscillatory type. Other parameter values are $q=-2.0$, $\gamma_+=0.01, \gamma_-=0.5$.

critical frequency Ω_c on D and Γ for different q. Note that the oscillations will set in with a finite frequency at both transitions from $\Omega_c=0$ to $\Omega_c>0$.

IV. EFFECTS IN THE WEAKLY NONLINEAR REGIME

We now turn to a discussion of the behavior of the system beyond linear stability analysis. Our discussion will be restricted to stationary patterns. A more detailed analysis of oscillatory patterns will be given elsewhere [17].

In the vicinity of the critical control parameter η_c and the critical wave number k_c, the linear dispersion of the slow mode $\omega_+(\eta,k^2)$ may be expanded to obtain the linear part of a nonlinear evolution equation for the slow mode near the bifurcation point. From Eq. (11) one gets

$$\omega_+(\eta,k^2)=k^{z_a-2}\tau_a^{-1}\left\{\frac{\eta-\eta_c}{\eta_c}+\xi_a^2(k-k_c)^2 + O[(k-k_c)^4]\right\}, \tag{17}$$

where $z_a=4$ for soft-mode instabilities ($a=s$) and $z_a=2$ for hard-mode instabilities ($a=h$). The expressions for time scales τ_a and length scales ξ_a can be found in Appendix A for soft mode instabilities and in Appendix B for hard-mode instabilities.

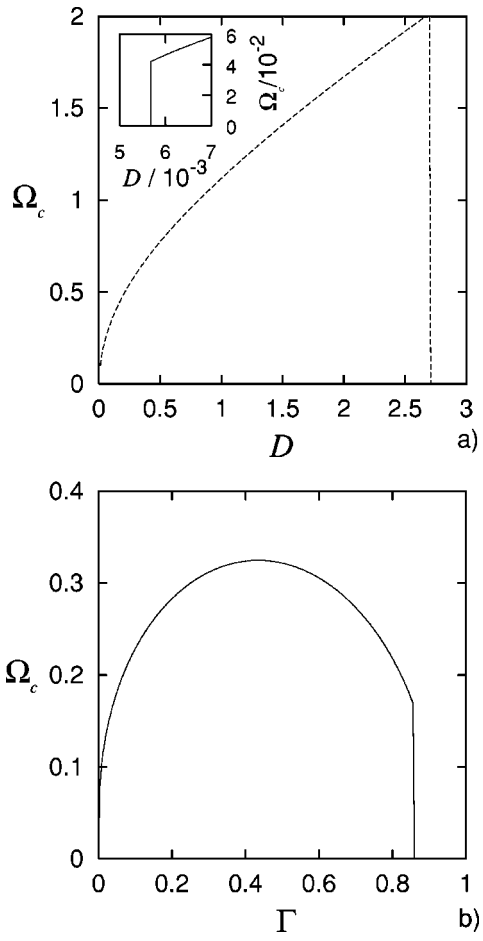

FIG. 5. (a) The critical frequency Ω_c as a function of D for $\Gamma=0.51$ with $q=-5$. The inset shows that Ω_c jumps to zero discontinuously. (b) Ω_c as a function of Γ for $D=0.09$ with $q=-2$. The remaining parameter is $\gamma_+-\gamma_-=-0.49$ for both (a) and (b).

A. Soft-mode instabilities

To proceed beyond the linearized dynamics near a soft-mode instability, it is convenient to introduce the variable $u=(\gamma_+\varrho+\gamma_-\zeta)/\Gamma$, which corresponds to fluctuations of the total channel density $u=(n_o+n_c-\overline{n})/\overline{n}$ and which contains the critical slow mode as $\eta\to\eta_c$. Furthermore, we introduce $v=(\varrho-\zeta)/\Gamma$, which remains fast relative to u near the bifurcation. We get an equation for the slowly varying part of $u(\mathbf{r},t)$ from a gradient expansion, which is outlined in Appendix A.

If we take into account all terms of $O(\nabla^2)$ and include the $O(\nabla^4)$ terms, which arise from the linear dispersion Eq. (17), the resulting equation for u takes on the form of a dynamical Cahn-Hilliard equation (or "model B") [18],

$$\partial_t u=\tau_s^{-1}\nabla^2\left\{\frac{\delta F(u)}{\delta u}\right\}+O(\nabla^4u^2). \tag{18}$$

with an effective potential $F(u)=\int[f(u)+(\xi_s^2/2)(\nabla u)^2]d^2\mathbf{r}$.

The local part $f(u)$ is given by

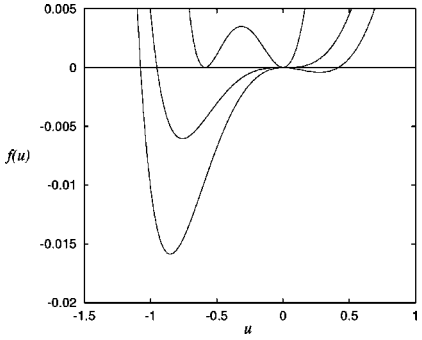

FIG. 6. Local part of the effective potential $f(u)$, which controls the Cahn-Hilliard dynamics near soft-mode instabilities at $\alpha=0.6$. The uppermost curve displays the situation at the transition ($\eta_c/\eta=1.025\,25$), whereas the middle curve corresponds to the spinodal point $\eta_c/\eta=1$. The lower curve is in the supercritical regime at $\eta_c/\eta=0.97$. For better visibility, $f(u)$ at the transition point has been enlarged by a factor of 10. If $\alpha<0.5$ the global minimum of the potential is attained for positive u and the graphs appear mirrored at the $u=0$ axis.

$$f(u)=\frac{\eta_c u^2}{2}+\frac{\eta}{\alpha^2}\left[(2-\alpha)u+\left(1-\frac{2}{\alpha}-u\right)\ln(1+\alpha u)\right], \tag{19}$$

with α as introduced in Eq. (8). Equation (18) has to be solved under the constraint of conservation of channel number, $\int u d^2\mathbf{r}=0$, which may be taken into account by an appropriate Lagrange multiplier term $-\Lambda u$ in $f(u)$. Note that the dynamics only depends on the ratio η_c/η and on the parameter α. It thus exhibits a particularly simple universality for all permissible values of $D, q, \gamma_{\pm}$.

Figure 6 shows the effective potentials for $\alpha=0.6$ close to the transition. The critical point η_c becomes the spinodal. In the subcritical regime $\eta<\eta_c$, $f(u)$ develops a second minimum $u_1\neq 0$, which decreases with increasing η. For $\eta>\eta_T$ with $u_1(\eta_T)=0$, a quench of the homogeneous state $u=0$ will result in nucleation and decomposition of the homogeneous state up to the spinodal point $\eta=\eta_c$. For $\eta>\eta_c$ the homogeneous state decays by spinodal decomposition.

The discussion of the dynamical behavior, including typical coarsening in the case of quenches, can be found in standard textbooks; see, for instance, [19].

B. Hard-mode instabilities

In order to obtain an analytic description of the weakly nonlinear regime for hard-mode instabilities, we use a standard multiscale perturbative approach, which results in an amplitude equation [20]. The approach starts from the ansatz

$$\mathbf{u}_c[\chi(X,Y,T)e^{ik_c x}+\chi^*(X,Y,T)e^{-ik_c x}] \tag{20}$$

for the fluctuations $\mathbf{u}=(\varrho,\zeta,\Phi)$. The amplitude χ depends upon the scaled variables $X=ax$, $Y=a^{1/2}y$, and $T=a^2t$. The scale a becomes small, if the control parameter η approaches its critical value η_c from above, $a^2=(\eta-\eta_c)/\eta_c$. For convenience we sketch the procedure in Appendix B. For one-dimensional, stationary patterns the perturbation theory gives the following for the amplitude χ in the supercritical vicinity of η_c:

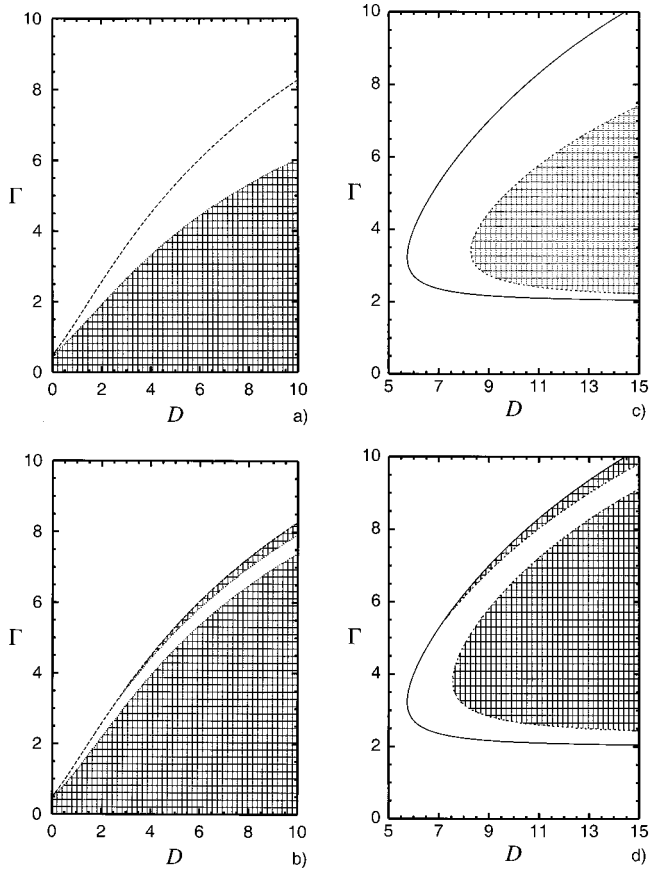

FIG. 7. $J=0$ lines within the $k_c^2\geqslant 0$ domain for $q=0.1$ and various α and γ : (a) $\alpha=0.25$, $\gamma=-0.49$; (b) $\alpha=0.75$, $\gamma=-0.49$; (c) $\alpha=0.25$, $\gamma=2.0$; and (d) $\alpha=0.75$, $\gamma=2.0$. The values of α and γ crucially determine the number and geometry of domains with continuous transitions (shaded).

$$\tau_h\partial_t\chi=\frac{\eta-\eta_c}{\eta_c}\chi+\xi_h^2\left[\partial_x-\frac{i}{2k_c}\partial_y^2\right]^2\chi-J|\chi|^2\chi. \tag{21}$$

The lengthy expression for the coupling constant J as a function of the model parameters is given in Appendix B.

Figure 7 displays the sign of J in the D-Γ plane for fixed $q=0.1$. Positive J corresponds to a continuous transition and (forward bifurcation) negative J corresponds to a discontinuous one (backward bifurcation). The shapes of the regions with different signs of J depend crucially on the parameters α [compare Fig. 7(a) with Fig. 7(b) and Fig. 7(c) with Fig. 7(d)] and γ [compare Fig. 7(a) with Fig. 7(c) and Fig. 7(b) with Fig. 7(d)].

Note that for $\alpha\leqslant 0.5$ [Figs. 7(a) and 7(c)] there is only one interval of positive J both for fixed D and for fixed Γ, whereas in the other regime $\alpha>0.5$ [Figs. 7(b) and 7(d)] there may be two such intervals and the domain of $J>0$ consists of two disconnected parts that extend to the ($k_c^2=0$) line in the considered region of parameters. This means that coming from large values of D, one leaves the area of

continuous transitions, crosses the domain of discontinuous transitions, and again enters a domain with $J>0$ before finally the $k_c^2=0$ line is crossed. The same behavior is obtained by changing Γ at a given D.

For negative γ the region of $J\geqslant 0$ contains the D axis. For positive γ, $k_c^2<0$ for small Γ.

V. CONCLUSIONS

We have studied a simple model of spontaneous pattern formation of mobile ions in a fluid membrane. The channel proteins may switch between an open and a closed state according to a simple two-state reaction kinetics with constant rates. The effective electrophoretic charge and the diffusion constant of the channel proteins are assumed to be state dependent. The reversal potential E of ions, which may pass the open channels constitutes a nonequilibrium driving force. The characterization of a particular model is completed by the additional parameters $D=D_c/D_o$ and $q=q_c/q_o$, the reaction rates $\gamma_\pm$, and the parameter α, which is the part of transmembrane conductivity due to open channels. Varying these parameters leads to a number of distinct scenarios for the first bifurcations from the stationary and homogeneous state. Depending on the sign of the control parameter $\eta=\alpha(\alpha-1)\beta q_o E$ and the ratio $q=q_c/q_o$ of electrophoretic charges, four qualitatively different regions of parameters have been identified from linear stability analysis: (a) for $q>0$ and $\eta>0$ ($\mathcal{R}_{++}$) soft- or hard-mode instabilities leading to stationary patterns will appear, (b) for $q<0$ and $\eta<0$ ($\mathcal{R}_{--}$) only bifurcations with soft-mode instabilities can occur, (c) for $q<0$ and $\eta>0$ ($\mathcal{R}_{-+}$) hard-mode instabilities with or without temporal oscillations may be found, and (d) for $q>0$ and $\eta<0$ ($\mathcal{R}_{+-}$) the homogeneous, stationary state remains linearly stable. In the fast reaction limit, where the time scale Γ^{-1} becomes much shorter than other time scales (except the RC-relaxation time of transmembrane potential fluctuations), only soft-mode instabilities remain. By varying the ratio $D=D_c/D_o$ of diffusion constants or $q=q_c/q_o$ of effective electrophoretic charges within physiologically plausible bounds, it is possible to switch between soft- and hard-mode instabilities in $\mathcal{R}_{++}$ and between hard-mode and oscillatory instabilities in $\mathcal{R}_{-+}$.

For soft-mode instabilities, we have derived an equation of motion of slow modes near the transition, which is of the form of a dynamical Cahn-Hilliard equation. The transition will generically be discontinuous (backward bifurcation) and the nonlinear evolution will be characterized by regions of nucleation and of spinodal decomposition. Quenches into the supercritical regime are predicted to show coarsening behavior with a coarsening length scale growing as $t^{1/3}$. For hard-mode instabilities, an amplitude equation is obtained as in [2] and parameter regions of forward and backward bifurcations may be distinguished by the sign of the nonlinear coupling parameter.

The presented model includes and extends several previously studied models and may be considered as a minimal model for charged ion channels with internal state kinetics in a fluid membrane.

APPENDIX A: GRADIENT EXPANSION NEAR SOFT-MODE INSTABILITIES

We transform Eqs. (6)–(8) to the new variables

$$u=(\gamma_+\varrho+\gamma_-\zeta)/\Gamma,$$
$$v=(\varrho-\zeta)/\Gamma \tag{A1}$$

and get

$$\Gamma\partial_t u=(\gamma_++D\gamma_-)\nabla^2 u+\gamma_+\gamma_-(1-D)\times\nabla^2 v+(\gamma_++r\gamma_-)\nabla^2\Phi+(\gamma_++r\gamma_-)\times\boldsymbol{\nabla}\cdot(u\boldsymbol{\nabla}\Phi)+\gamma_+\gamma_-\boldsymbol{\nabla}\cdot(v\boldsymbol{\nabla}\Phi) \tag{A2}$$

as the equation of motion for u. Note that all terms on the rhs of the equation for u are at least $O(\nabla^2)$ as a direct consequence of channel-number conservation. For v we get

$$\Gamma\partial_t v=-\Gamma^2 v+(\gamma_-+D\gamma_+)\nabla^2 v+(1-D)\times\nabla^2 u+(1-r)\nabla^2\Phi+(1-r)\boldsymbol{\nabla}\cdot(u\boldsymbol{\nabla}\Phi)+(\gamma_-+r\gamma_+)\boldsymbol{\nabla}\cdot(v\boldsymbol{\nabla}\Phi). \tag{A3}$$

Note that v decays with a rate $O(\nabla^0)$ due to the $-\Gamma^2 v$ term. Thus v is fast near a soft-mode transition and may be adiabatically eliminated. It does not enter the leading order of the gradient expansion, which is obtained by replacing Φ in Eq. (A2) from the leading $[O(\nabla^0)]$ order of

$$0=(1-\nabla^2)\Phi+\eta(u+\gamma_- v)+\alpha(u+\gamma_- v)\Phi. \tag{A4}$$

This leads to

$$\partial_t u=\tau_s^{-1}\nabla^2\left\{\eta_c u+(1+u)\phi(u)-\int\phi(u)\,du\right\} \tag{A5}$$

with $\tau_s^{-1}=(\gamma_++D\gamma_-)/\Gamma$ and $\phi(u)=-\eta u/(1+\alpha u)$.

The linear $O(\nabla^4)$ term is obtained from the expansion of $\omega_+(\eta,k^2)=\tau_s^{-1}k^2[(\eta-\eta_c)/\eta_c+\xi_s^2+O(k^4)]$. For ξ_s^2/τ_s we obtain

$$\frac{\xi_s^2}{\tau_s}=-\frac{\eta}{2}+\frac{1}{4\Gamma}[(1-D-\eta)^2+2\eta(\gamma_--\gamma_+)-4\eta\gamma_- Dq]-\frac{1}{4\Gamma^3}[(\gamma_--\gamma_+)(1-D-\eta)+2\eta\gamma_- Dq]^2. \tag{A6}$$

Adding a term $-\tau_s^{-1}\xi_s^2\nabla^4 u$ on the rhs of Eq. (A5) we get Eqs. (18) and (19).

APPENDIX B: AMPLITUDE EQUATION NEAR HARD-MODE INSTABILITIES

The system of nonlinear partial differential equations Eqs. (6)–(8) is written as $\mathcal{L}\mathbf{u}=\mathcal{N}(\mathbf{u},\mathbf{u})$ In the vicinity of η_c, k_c, $\mathbf{u}=(\varrho,\zeta,\Phi)$ contains both fast scale variations [with $\boldsymbol{\nabla}u=O(k_c)$] and slow scale variations (with $\boldsymbol{\nabla}u\to 0$ for $\eta\to\eta_c$). The slowly varying part may be obtained from a perturbation expansion in $\epsilon=\sqrt{|(\eta-\eta_c)/\eta_c|}$, which explic-

itly separates slow scale variations from fast scales by introducing appropriately scaled length and time variables $X=\epsilon x$ $T=\epsilon^2 t$. For one-dimensional patterns, the direction perpendicular to the pattern wave vector should be scaled as $Y=\epsilon^{1/2}y$ [21]. As the functions now may depend upon fast and slow variables, we have to replace $\partial_t \rightarrow \partial_t+\epsilon^2\partial_T$ and $\partial_x \rightarrow \partial_x+\epsilon\partial_X$, etc. In this way, the linear part $\mathcal{L}$ becomes $\mathcal{L}=\mathcal{L}_0+\epsilon\mathcal{L}_1+\epsilon^2\mathcal{L}_2$. Inserting the expansion $\mathbf{u}=\epsilon\mathbf{u}_1+\epsilon^2\mathbf{u}_2+\epsilon^3\mathbf{u}_3+O(\epsilon^4)$ [with $\mathbf{u}_1(X,Y,T,x)=\chi(X,Y,T)\exp(ik_c x)+\mathrm{cc}$] and sorting with respect to powers of ϵ one gets a hierarchy of equations, which allows to determine $\mathbf{u}_n$ from the $\mathbf{u}_k$ with $k<n$. It starts with $\mathcal{L}_0\mathbf{u}_1=0$, which implies that $\mathbf{u}_1$ is an eigenstate to $\mathcal{L}_0$ with eigenvalue zero. As ∂_T carries an explicit factor of ϵ^2, the equation, that contains the slow time derivative of $\mathbf{u}_1$ appears in third order in ϵ and has the form $\mathcal{L}_2\mathbf{u}_1+\mathcal{L}_1\mathbf{u}_2+\mathcal{L}_0\mathbf{u}_3=\mathcal{N}_3(\mathbf{u}_1,\mathbf{u}_2)$. After inserting $\mathbf{u}_2$ as obtained from the perturbation expansion in terms of $\mathbf{u}_1$, one gets the amplitude equation by taking the scalar product of the third order equation with the left eigenstate of $\mathcal{L}_0$ to eigenvalue zero, $\mathbf{u}_1^\dagger$. This solvability condition gives

$$\int \mathbf{u}_1^\dagger\mathcal{L}_2\mathbf{u}_1 d^2\mathbf{r}+\int \mathbf{u}_1^\dagger\mathcal{L}_1\mathbf{u}_2 d^2\mathbf{r}=\int \mathbf{u}_1^\dagger\mathcal{N}_3 d^2\mathbf{r}. \quad \text{(B1)}$$

The lhs of Eq. (B1) is linear in χ and can be obtained directly from expanding $\omega_+(\eta,k^2)$ around η_c,k_c, $\omega_+(\eta,k^2)=\tau_h^{-1}(\epsilon^2+\xi_h^2(k-k_c)^2+O[(k-k_c)^4])$. Inserting this expansion on the lhs of Eq. (B1) and neglecting the y dependence for simplicity gives

$$\left(\tau_h\partial_t-\frac{\eta-\eta_c}{\eta_c}-\xi_h^2\partial_x^2\right)\chi=\int \mathbf{u}_1^\dagger\mathcal{N}_3 d^2\mathbf{r}. \quad \text{(B2)}$$

For the time constant τ_h we get

$$\tau_h=\frac{\Gamma+(1+D)k_c^2-\eta_c k_c^2/(1+k_c^2)}{Dk_c^2(k_c^2+\gamma_-+\gamma_+/D)} \quad \text{(B3)}$$

and the square of the correlation length ξ_h^2 is

$$\xi_h^2=\frac{4k_c^2}{(1+k_c^2)\left(k_c^2+\gamma_-+\dfrac{\gamma_+}{D}\right)}. \quad \text{(B4)}$$

Evaluating the nonlinear term on the rhs of Eq. (B2) gives Eq. (21) with the following expression for J:

$$\begin{aligned}J=&\frac{-\eta_c}{\left(k_c^2+\gamma_-+\dfrac{\gamma_+}{D}\right)(1+k_c^2)^2}\left\{\alpha\left(q\gamma_-+\frac{\gamma_+}{D}+k_c^2\right)\right.\\&\times(p_1+\Phi_{k_c}n_1+2\alpha)-(1+k_c^2)\\&\times\left[2p_1\left(\frac{\gamma_+}{D}+k_c^2+\zeta_{k_c}q\gamma_-\right)-\Phi_{k_c}\{n_1(\gamma_++k_c^2)\right.\\&\left.\left.-q\gamma_-(1+k_c^2)z_1\}\right]\right\}.\end{aligned}$$

The expressions n_1,z_1, and p_1 stem from $O(\epsilon^2)$ corrections and have the form

$$\begin{aligned}n_1=&\frac{1}{18k_c^4}\{(1+4k_c^2)(\gamma_+/D+4k_c^2+\zeta_{k_c}q\gamma_-)\\&-2\alpha(\gamma_++q\gamma_-+4k_c^2)\},\end{aligned} \quad \text{(B5)}$$

$$z_1=\frac{n_1(\beta+2k_c^2)(1+4k_c^2)+4k_c^2(\alpha-n_1\eta_c)}{\beta(1+4k_c^2)(1+k_c^2)}, \quad \text{(B6)}$$

$$p_1=\frac{(1+k_c^2)En_1+\alpha}{1+4k_c^2}. \quad \text{(B7)}$$

[1] L.F. Jaffe, Nature (London) **265**, 600 (1977).
[2] P. Fromherz and W. Zimmermann, Phys. Rev. E **51**, 1659 (1995).
[3] L.P. Savtchenco and S.M. Korogod, Neurophysiology **26**, 99 (1994).
[4] M. Léonetti and E. Dubois-Violette, Phys. Rev. E **56**, 4521 (1997).
[5] F.M. Harold and J.H. Caldwell, in *Tip Growth in Plant and Fungal Cells*, edited by I.B. Heath (Academic, New York, 1990).
[6] E.R. Kandel and J.H. Schwartz, *Principles of Neural Science*, 2nd ed. (Elsevier, New York, 1985).
[7] S. Leibler, J. Phys. (Paris) **47**, 507 (1986).
[8] M. Goulian, R. Bruinsma, and P. Pincus, Europhys. Lett. **22**, 145 (1993).
[9] P. Fromherz, Ber. Bunsen. Phys. Chem. **92**, 1010 (1988).
[10] M. Léonetti and E. Dubois-Violette, Phys. Rev. Lett. **81**, 1977 (1998).
[11] M. Léonetti, Eur. Phys. J. B **2**, 325 (1998).
[12] B. Hille, *Ionic Channels of Excitable Membranes*, 2nd ed. (Sinauer Associates, Sunderland, 1992).
[13] D.J. Aidley and P.R. Stansfield, *Ion Channels: Molecules in Action* (Cambridge University Press, Cambridge, England, 1996).
[14] D.L. Nelson and M.M. Fox, in *Lehninger: Principles of Biochemistry*, 3rd ed. (Worth, New York, 2000).
[15] H.B. Peng and M. Poo, Trends Neurosci. **9**, 125 (1986).
[16] P. Fromherz, Biochim. Biophys. Acta **944**, 108 (1988).
[17] S.C. Kramer and R. Kree (unpublished).
[18] P.C. Hohenberg and B.I. Halperin, Rev. Mod. Phys. **49**, 435 (1977).
[19] P.M. Chaikin and T.C. Lubensky, *Principles of Condensed Matter Physics* (Cambridge University Press, Cambridge, 1995).
[20] M.C. Cross and P.C. Hohenberg, Rev. Mod. Phys. **65**, 851 (1993).
[21] A.C. Newell and J.A. Whitehead, J. Fluid Mech. **38**, 279 (1969).